



## Forcing of western tropical South Atlantic sea surface temperature across three glacial-interglacial cycles

Alicia Hou<sup>a,\*</sup>, André Bahr<sup>a</sup>, Stefan Schmidt<sup>a</sup>, Cornelia Strebl<sup>a</sup>, Ana Luiza Albuquerque<sup>b</sup>, Cristiano M. Chiessi<sup>c</sup>, Oliver Friedrich<sup>a</sup>

<sup>a</sup> Institute of Earth Sciences, Heidelberg University, Heidelberg, Germany

<sup>b</sup> Programa de Geociências (Geoquímica), Universidade Federal Fluminense, Niterói, Brazil

<sup>c</sup> School of Arts, Sciences and Humanities, University of São Paulo, São Paulo, Brazil

### ARTICLE INFO

#### Keywords:

Western tropical Atlantic  
Sea surface temperature  
Southeast trade winds  
Marine Isotope Stage 6  
Zonal temperature gradient  
Meridional temperature gradient

### ABSTRACT

The western tropical Atlantic (WTA) supplies warm and saline waters to the upper-limb of the Atlantic Meridional Overturning Circulation (AMOC) and may store excess heat and salinity during periods of AMOC slowdown. Since previous sea surface temperature (SST) reconstructions from the WTA typically focus on the Last Glacial Maximum and the last deglaciation, additional long-term records spanning multiple glacial-interglacial transitions are needed in order to elucidate the drivers of long-term WTA SST variability. We performed Mg/Ca analyses on the surface-dwelling planktic foraminifera *Globigerinoides ruber* (pink) from a sediment core raised from the southern WTA to reconstruct SST changes over the past 322 kyr. We evaluate the relative importance of atmospheric  $p\text{CO}_2$ , AMOC strength and trade-wind intensity in driving the thermal evolution of the WTA across three glacial-interglacial cycles. Our results indicate a lack of pronounced glacial-interglacial variability in the SST record, prompting us to exclude atmospheric  $p\text{CO}_2$  as a direct driver of SST variations in the southern WTA. Similarly, we conclude that variations in AMOC strength also likely did not have a strong influence on long-term WTA SST, based on the low and relatively stable interhemispheric SST gradient over the past 322 kyr. Our results reveal high-amplitude variability in zonal SST gradients within the (sub)tropical South Atlantic and similarities between the long-term patterns of the intrahemispheric meridional SST gradient and our SST record. Based on these findings, we propose that changes in the intrahemispheric meridional SST gradient modulate southeast trade wind intensity, which in turn drives variations in zonal SST gradients and southern WTA SSTs.

### 1. Introduction

The western tropical Atlantic (WTA) is the major source of heat and salinity for the northward-flowing surface branch of the Atlantic Meridional Overturning Circulation (AMOC). A number of modelling studies have demonstrated that a sluggish northward heat transport during phases of weak AMOC causes warm water masses to accumulate in the WTA (particularly south of the equator), resulting in anomalous SST warming (Chang et al., 1997; Dahl et al., 2005; Vellinga and Wood, 2002; Yang, 1999). This suggests that the surface layer of the WTA may function as an important reservoir for excess heat and salinity when northward heat transport is reduced. Paleoclimate reconstructions of the last deglaciation reveal that when the AMOC was in an “off” mode (e.g., Heinrich Stadial 1) (Böhm et al., 2015), millennial-scale warming

events occurred in the tropical and subtropical latitudes of the South Atlantic western boundary (Chiessi et al., 2015; Rühlemann et al., 1999; Weldeab et al., 2006), while concurrent cooling occurred in the midlatitude North Atlantic (Bard et al., 2000). These proxy studies thus confirm the ability of the western tropical and subtropical South Atlantic to store surplus heat during abrupt phases of severe AMOC weakening (Chiessi et al., 2015; Weldeab et al., 2006).

While the ability of the WTA to respond to AMOC disruptions by storing excess heat is well-documented for Heinrich Stadial 1 (Arz et al., 1999; Chiessi et al., 2015; Rühlemann et al., 1999; Weldeab et al., 2006), there is a shortage of long-term records encompassing several glacial/interglacial cycles. Hence, it is uncertain whether glacial-interglacial variations in the strength of the AMOC (i.e., heat export to the North Atlantic) played an important role in the long-term thermal

\* Corresponding author.

E-mail addresses: [alicia.hou@geow.uni-heidelberg.de](mailto:alicia.hou@geow.uni-heidelberg.de) (A. Hou), [andre.bahr@geow.uni-heidelberg.de](mailto:andre.bahr@geow.uni-heidelberg.de) (A. Bahr), [Strebl@stud.uni-heidelberg.de](mailto:Strebl@stud.uni-heidelberg.de) (C. Strebl), [ana\\_albuquerque@id.uff.br](mailto:ana_albuquerque@id.uff.br) (A.L. Albuquerque), [chiessi@usp.br](mailto:chiessi@usp.br) (C.M. Chiessi), [Oliver.Friedrich@geow.uni-heidelberg.de](mailto:Oliver.Friedrich@geow.uni-heidelberg.de) (O. Friedrich).

<https://doi.org/10.1016/j.gloplacha.2020.103150>

Received 27 August 2019; Received in revised form 20 February 2020; Accepted 27 February 2020

Available online 29 February 2020

0921-8181/ © 2020 Elsevier B.V. All rights reserved.

evolution of the southern WTA or if other climatic processes were more influential at these timescales. There is documented evidence of prolonged SST warming in the western subtropical South Atlantic during the penultimate and last glacials in response to a glacial-weakening of the AMOC (Santos et al., 2017). However, this SST record is likely not representative for the tropics as it may be influenced by the northward intrusion of water masses from the mid-latitude Brazil-Malvinas Confluence (Campos et al., 1996; Santos et al., 2017). Additionally, given that past upwelling at this study site has been of comparable intensity to the most important upwelling zone along the coast of southeastern Brazil, SST variations observed at this locality may reflect a local signal (Lessa et al., 2017, 2019). As such, it remains unknown whether a glacial reduction of the overturning circulation can likewise produce significant surface changes in the tropical latitudes of the western boundary. Previous SST records from the tropical oceans have shown a dominance of 100-kyr cycles attributed to glacial-interglacial variations in atmospheric CO<sub>2</sub> concentration (Herbert et al., 2010; Lea, 2004). Therefore, we would expect direct radiative forcing by CO<sub>2</sub> to have a similarly strong influence on SST in the southern WTA. In addition, glacial reductions in atmospheric pCO<sub>2</sub> have been shown to enhance the intra-hemispheric thermal gradient (Broccoli and Manabe, 1987), which in turn influence the intensity of tropical trade winds (Broccoli and Manabe, 1987; Mix et al., 1986; Rind, 1998). Glacial-interglacial variations in the strength of the southern hemisphere trade wind system are well-documented particularly from eastern boundary upwelling regions along the coast of Africa (Little et al., 1997a,b; Shi et al., 2001; Stuut et al., 2002). While a glacial intensification of the southern trades has been shown to produce cool SST anomalies along the eastern boundary, it is rather unclear if and how glacial-interglacial changes in their strength influences SST in the southern WTA.

An important consequence of surface hydrographic changes in the WTA are potential changes in the terrestrial hydroclimate of South America. Reconstructions of continental precipitation indicate that the build-up of excess heat in the southern WTA produced millennial-scale wet periods over the otherwise semi-arid northeastern Brazil via a southward displacement of the Intertropical Convergence Zone (ITCZ) (Mulitza et al., 2017; Wang et al., 2004). Hence, future SST changes in the WTA in response to global climate change may impact human societies and natural ecosystems in regions prone to drought, such as northeastern Brazil (Marengo and Bernasconi, 2015). In order to mitigate the potential negative consequences that may arise from WTA SST anomalies, it is of utmost societal and ecological importance to accurately predict how anthropogenic forcing (e.g. higher greenhouse gas concentrations) will affect WTA SST. Investigating the long-term thermal evolution of this region will provide information regarding the sensitivity of WTA SST to climatic perturbations, its modes of variability, as well as the major climatic drivers of WTA SST evolution. The lack of SST reconstructions of sufficient temporal length and resolution, particularly from the southern WTA sector, however, has thus far prevented a thorough investigation of the long-term thermal evolution of this region. Therefore, additional SST records spanning multiple glacial-interglacial intervals from the southern WTA are urgently needed.

Here, we present a 322-kyr, high-resolution SST reconstruction of the southern WTA, off the coast of eastern Brazil using planktic foraminiferal Mg/Ca ratios. The study site is ideally suited for reconstructing regional-scale oceanographic processes within the WTA as it is located within the western tropical Atlantic warm pool, away from zones of maximum upwelling on the Brazil margin (Castelao and Barth, 2006). To reconstruct surface ocean conditions in the southern WTA, we used the planktic foraminiferal species *Globigerinoides ruber* (pink) which lives in the upper mixed layer of the tropical and subtropical waters (Chiessi et al., 2007; Steph et al., 2009; Tolderlund and Bé, 1971). Using our new WTA SST record, we investigate the role of atmospheric pCO<sub>2</sub>, AMOC strength and Southern Hemisphere trade-wind intensity in WTA SST evolution across multiple glacial-interglacial cycles and propose a mechanism through which WTA SST responds to

climatic forcing.

## 2. Regional oceanographic and atmospheric setting

### 2.1. Hydrography of the western tropical South Atlantic

The surface mixed layer of the western tropical South Atlantic is bathed by warm, saline and oligotrophic Tropical Water ( $T > 20$  °C,  $S > 36.40$ ) (Castro et al., 2006; Stramma and England, 1999). At the study site, the modern annual mean SST and sea-surface salinity is  $26.02 \pm 0.51$  °C (Locarnini et al., 2013) and  $37.11 \pm 0.135$  (Zweng et al., 2013), respectively. The present-day amplitude of seasonal SST variability is  $\sim 3$  °C, with the warmest temperatures ( $27.62 \pm 0.30$  °C) occurring during the austral summer (January to March) and the coldest SST ( $24.34 \pm 0.10$  °C) occurring during austral winter (July to September) (Locarnini et al., 2013). Upper layer circulation at the site is mainly influenced by the Brazil Current (BC), which is the southward-flowing western boundary branch of the South Atlantic Subtropical Gyre (Peterson and Stramma, 1991). The BC originates at ca. 10°S when the zonally-oriented southern branch of the South Equatorial Current (sSEC) splits into a southward flowing current (BC) and a northward-flowing current (North Brazil Current; NBC) (Peterson and Stramma, 1991; Rodrigues et al., 2007; Stramma, 1991) (Fig. 1). Surface waters advected westward within the sSEC experience high radiative heating and are thus warm and saline (Hastenrath, 1980). Results from a modelling study indicate that BC transport responds to seasonal variability in the bifurcation latitude of the sSEC (Rodrigues et al., 2007). BC transport is maximized (minimized) during austral spring/summer (winter) when the ITCZ is displaced to the south (north) and the bifurcation of the sSEC is shifted northward (southward) (Rodrigues et al., 2007). Observational and modelling data also indicate that BC transport strengthens with increasing latitude, such that the BC is a substantially stronger current at subtropical latitudes than in the tropics (Schmid and Majumder, 2018; Stramma, 1989; Stramma et al., 1990).

### 2.2. Southeast (SE) trade winds

Seasonal changes in temperature and spatial heat distribution within the mixed layer of the tropical Atlantic are strongly dependent on seasonal variations in the intensity of the SE trade winds (Carton and Zhou, 1997). During austral winter, the SE trade winds are strengthened, intensifying coastal upwelling and promoting cold SST anomalies in the eastern (sub)tropical South Atlantic (Shannon and Nelson, 1996). At the same time, strong SE trade winds also increase the westward advection of warm water masses within the sSEC (Johns et al., 2002; Molinari, 1983), causing warm water masses to accumulate in the western basin (Hastenrath and Merle, 1987; Merle, 1980). This results in an enhanced east-west temperature contrast within the eastern (sub) tropical South Atlantic. The build-up of warm water masses in the WTA also deepens the thermocline, which further contributes to western basin warming (Hastenrath and Merle, 1987; Merle, 1980; Carton and Huang, 1994). In austral summer, the situation is reversed: weakened SE trade winds cause both eastern boundary upwelling and westward SEC transport to diminish, resulting in a low SST contrast between the eastern and western parts of the tropical South Atlantic.

### 2.3. Coastal upwelling off eastern Brazil

Upwelling of relatively cold, fresh and nutrient-rich South Atlantic Central Water (SACW) occurs along eastern Brazil due to variations in alongshore bottom topography, changes in coastline geometry and wind forcing (Franchito et al., 2008; Rodrigues and Lorenzetti, 2001). Seasonal intensification of western boundary coastal upwelling takes place during austral spring and summer when the prevailing winds are northeasterly (Aguilar et al., 2014). Major upwelling systems along the Brazilian margin include the intense Cabo Frio upwelling zone ( $\sim 23^{\circ}$ S)

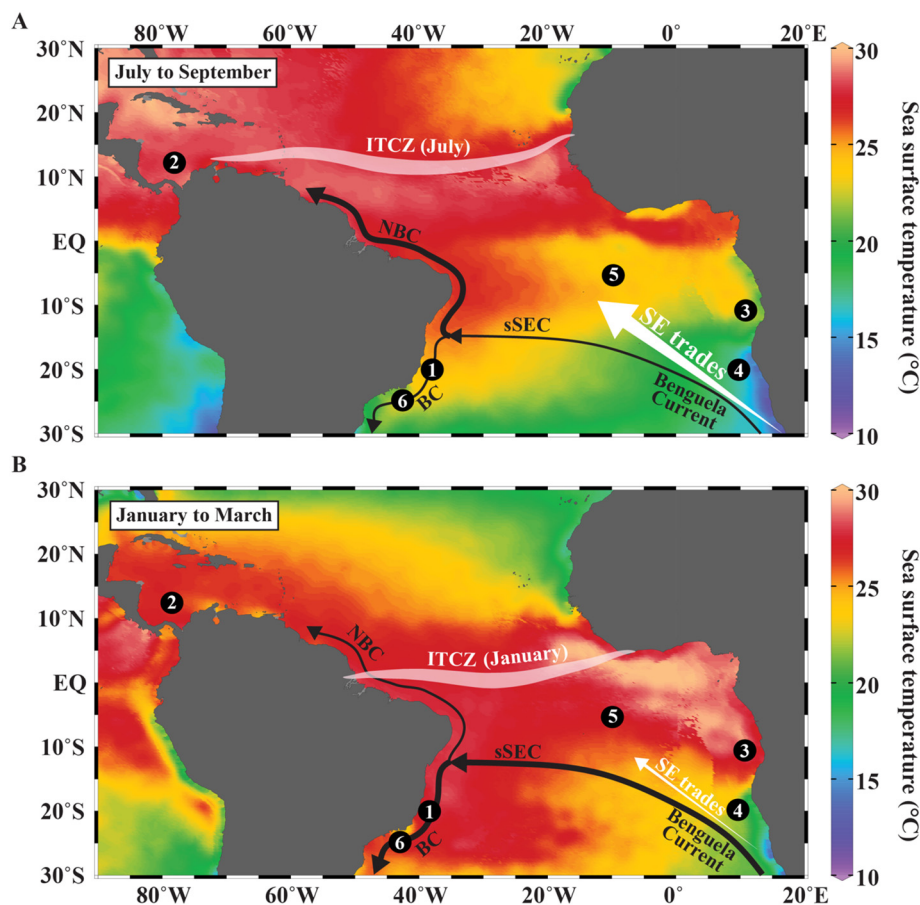


Fig. 1. Locations of cores (numbered black circles): (1) M125-55-7 and M125-55-8 (this study), (2) ODP Site 999 (Schmidt et al., 2006), (3) GeoB1016-3 (Schneider et al., 1995), (4) GeoB1028-5 (Schneider et al., 1995), (5) GeoB1112 (Nürnberg et al., 2000) and (6) GL-1090 (Santos et al., 2017). (A) Austral winter (July to September) average seasonal sea surface temperatures (colour shading) (Locarnini et al., 2013), configuration of major surface-ocean currents in the western tropical North and South Atlantic (black arrows; thickness of the arrows denotes the relative strengths of the currents) (Peterson and Stramma, 1991; Stramma and England, 1999), prevailing southeast (SE) trade winds (white arrow; thickness of arrow corresponds to relative wind intensity) and July latitudinal position of the Inter-tropical Convergence Zone (ITCZ) (white belt). (B) Austral summer (January to March) average seasonal sea-surface temperatures (Locarnini et al., 2013), positions of major surface-ocean currents (black arrows) (Peterson and Stramma, 1991; Stramma and England, 1999), the SE trades (white arrow) and January latitudinal position of the ITCZ (white belt). This figure was produced with Ocean Data View (Schlitzer, 2018).

Table 1 Results of <sup>14</sup>C analysis of core M125-55-7.

Depth (cm)	Planktic species	Lab ID	<sup>14</sup> C age (BP)	Uncertainty of <sup>14</sup> C age (years)	Calibrated age (kyr BP)
32.5	<i>G. ruber</i>	BE-9678.1.1	8059	30	8.5
47.5	<i>G. ruber</i>	BE-9679.1.1	10,067	37	11.1
70	<i>G. ruber</i>	BE-9680.1.1	12,244	37	13.7
120	<i>G. ruber</i>	BE-9681.1.1	36,879	511	41.1

Table 2 Tie points used to correlate the M125-55-7 benthic  $\delta^{18}\text{O}$  record to the LR04 benthic  $\delta^{18}\text{O}$  stack (Lisiecki and Raymo, 2005).

Continuous depth (cm)	Age (kyr BP)
190.0	64.0
296.1	86.0
420.0	108.0
431.3	118.3
475.6	131.1
567.5	165.0
584.0	190.7
605.2	198.6
664.4	208.3
695.0	219.1
740.1	226.1
763.3	232.8
791.2	243.8
815.3	254.4
884.8	267.3
919.3	280.2
1063.8	299.0
1162.2	317.0
1192.0	322.5

(Castelao and Barth, 2006) and the weaker Vitória Upwelling System (20–21°S) (Schmid et al., 2002), which is nearest to our study site.

### 3. Material and methods

#### 3.1. Piston core M125-55-7 and parallel multicore M125-55-8

Piston core M125-55-7 (1175 cm length) was retrieved from 1960.8 m water depth in March/April 2016 during R/V METEOR cruise M125. The coring site (20°21.807'S, 38°37.387'W) is located off eastern Brazil, close to the Rio Doce debouchment (Bahr et al., 2016) (Fig. 1). Core M125-55-7 consists of clay to silty clay with bioclasts with sediments varying between dark and light grey in colour without visible hiatus. Since the upper ~35 cm of core M125-55-7 was disturbed during coring, the parallel multicore M125-55-8 (44 cm length; same location) will be used for reconstruction of modern conditions. Multicore M125-55-8 consists of greyish-beige silt to medium-sized calcareous sand with abundant quartz, mica, heavy minerals, and shell debris (Bahr et al., 2016).

#### 3.2. Core sampling and selection of foraminifera

Omitting the disturbed core-top portion, 10 cm<sup>3</sup> of sediment was sampled from core M125-55-7 at approximately 2.5 cm resolution. Additionally, we collected two samples from multicore M125-55-8 at depths of 0–1 cm and 1–2 cm to retrieve modern hydrographic data. The samples were freeze-dried for 24 h and wet-sieved over a 63 μm mesh. The size-fractionated sediments were oven-dried overnight at 40 °C. Dried sediments were handpicked under a stereo microscope to select three benthic (*Uvigerina* spp.) and 30–40 planktic (*Globigerinoides ruber* pink) foraminifera specimens from each sample. Specimens were preferably picked exclusively from the > 315 μm size fraction to

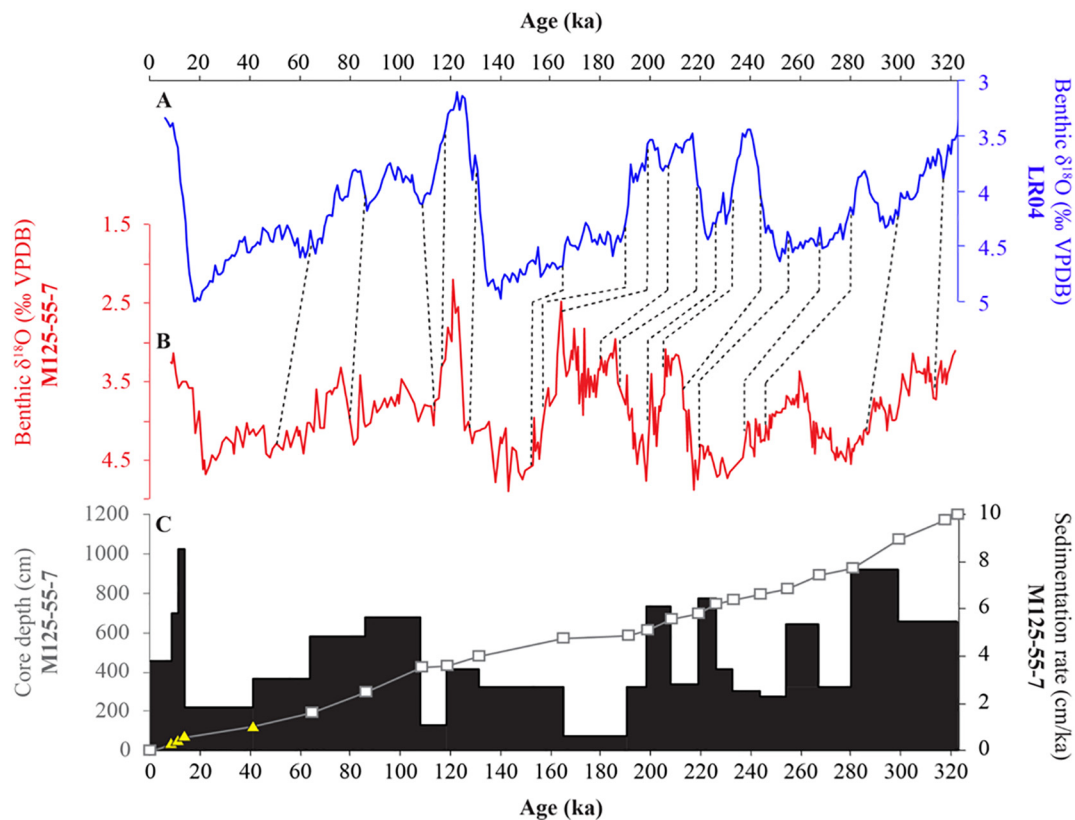


**Fig. 2.** Age model of core M125-55-7 derived from tuning its benthic foraminifera  $\delta^{18}\text{O}$  record to the LR04 benthic stack and calibrated radiocarbon ages. The uncertainties of the  $^{14}\text{C}$  dates are smaller than the symbol sizes (see Table 1). (A) LR04 benthic foraminifera  $\delta^{18}\text{O}$  stack (Lisiecki and Raymo, 2005) (blue line). (B) Core M125-55-7 benthic foraminifera  $\delta^{18}\text{O}$  record based on *Uvigerina* spp. (red line). Tie-points from tuning are indicated by the black dotted lines. (C) Core M125-55-7 age-depth model (grey line) and sedimentation rates (step plot, black shading). The yellow triangles denote the calibrated radiocarbon ages and the grey squares denote the tie points derived from tuning (Tables 1 and 2). (For interpretation of the references to colour in this figure legend, the reader is referred to the web version of this article.)

minimize size-dependent variability in shell geochemistry (Elderfield et al., 2002; Friedrich et al., 2012). A total of 11 samples did not have enough specimens in the  $> 315\ \mu\text{m}$  size range, so specimens from the  $250\text{--}315\ \mu\text{m}$  size fraction were also used. Foraminiferal tests were gently crushed between two glass plates to expose shell chambers prior to chemical treatment for geochemical analyses. Note that only the cleanest fraction of cracked tests was used for Mg/Ca analysis.

### 3.3. Stable-isotope analysis of benthic foraminifera

Cracked foraminiferal tests were rinsed three times with ultra-pure methanol and briefly ultrasonicated between washes. Stable isotopes were measured with a ThermoFinnigan MAT 253plus mass spectrometer coupled to a Kiel IV carbonate preparation line at the Institute of Earth Sciences, Heidelberg University (Germany). Measurements were calibrated to an in-house carbonate standard (Solnhofen limestone). Analytic precision based on repeated measurements of the in-house standard is  $0.06\text{‰}$  for  $\delta^{18}\text{O}$ .

### 3.4. *Globigerinoides ruber* (pink) Mg/Ca analysis

Chemical cleaning of crushed *G. ruber* (pink) tests prior to Mg/Ca analysis was performed under trace-metal free conditions in the clean-lab facilities at the Institute of Earth Sciences, Heidelberg University (Germany). The cleaning procedure involved oxidative and reductive steps following the protocol described in Martin and Lea (2002), omitting the final step of chelation with DTPA (Schmidt et al., 2006; Weldeab et al., 2006). Briefly, crushed *G. ruber* (pink) tests were first rinsed three times with ultra-pure water and methanol to remove fine

clay particles. The rinsed tests were then treated for 30 min with a reducing hydrazine/ammonium citrate solution for the removal of metal oxides. Afterwards, samples were transferred to new acid-leached vials. Finally, tests were treated for 20 min with an oxidizing NaOH-buffered  $\text{H}_2\text{O}_2$  solution to remove organic matter. The fully cleaned samples were subsequently leached in  $0.001\ \text{N}\ \text{HNO}_3$  prior to dissolution with  $0.1\ \text{N}\ \text{HNO}_3$ . The dissolved samples were diluted and analyzed with an Agilent 720 ICP-OES at the Institute of Earth Sciences, Heidelberg University (Germany). To monitor instrumental drift, an internal standard of  $20\ \text{ppm}\ \text{Ca}$  was measured after every 11 samples. *Globigerinoides ruber* (pink) Mg/Ca ratios were subsequently converted into SST using the Mg/Ca temperature relationship of Dekens et al. (2002) [ $\text{Mg}/\text{Ca} = 0.38 \exp. 0.09 \cdot \text{SST}$ ], as this calibration includes tropical Atlantic samples and sample preparation followed the same cleaning protocol involving a reductive cleaning step. Replicate runs yielded a mean reproducibility of  $\pm 0.34\ \text{mmol/mol}$  ( $\pm 0.92\ \text{°C}$ ).

### 3.5. Age model

The age model for core M125-55-7 was developed using  $^{14}\text{C}$ -based ages and tie points generated from tuning our benthic  $\delta^{18}\text{O}$  record to the LR04 benthic  $\delta^{18}\text{O}$  stack (Lisiecki and Raymo, 2005) using the AnalySeries 2.0.8 program (Paillard et al., 1996). For  $^{14}\text{C}$  dating, four samples were selected from the upper 120 cm of the core. Each sample consisted of approximately 300 tests of *G. ruber* (pink and white varieties), collected from the  $> 315\ \mu\text{m}$  size fraction. The samples were dated by accelerator mass spectrometry (AMS)  $^{14}\text{C}$  analysis in the LARA Laboratory of the University of the Bern (Switzerland) (Szidat et al., 2014; Gottschalk et al., 2018). The  $^{14}\text{C}$  ages were converted into

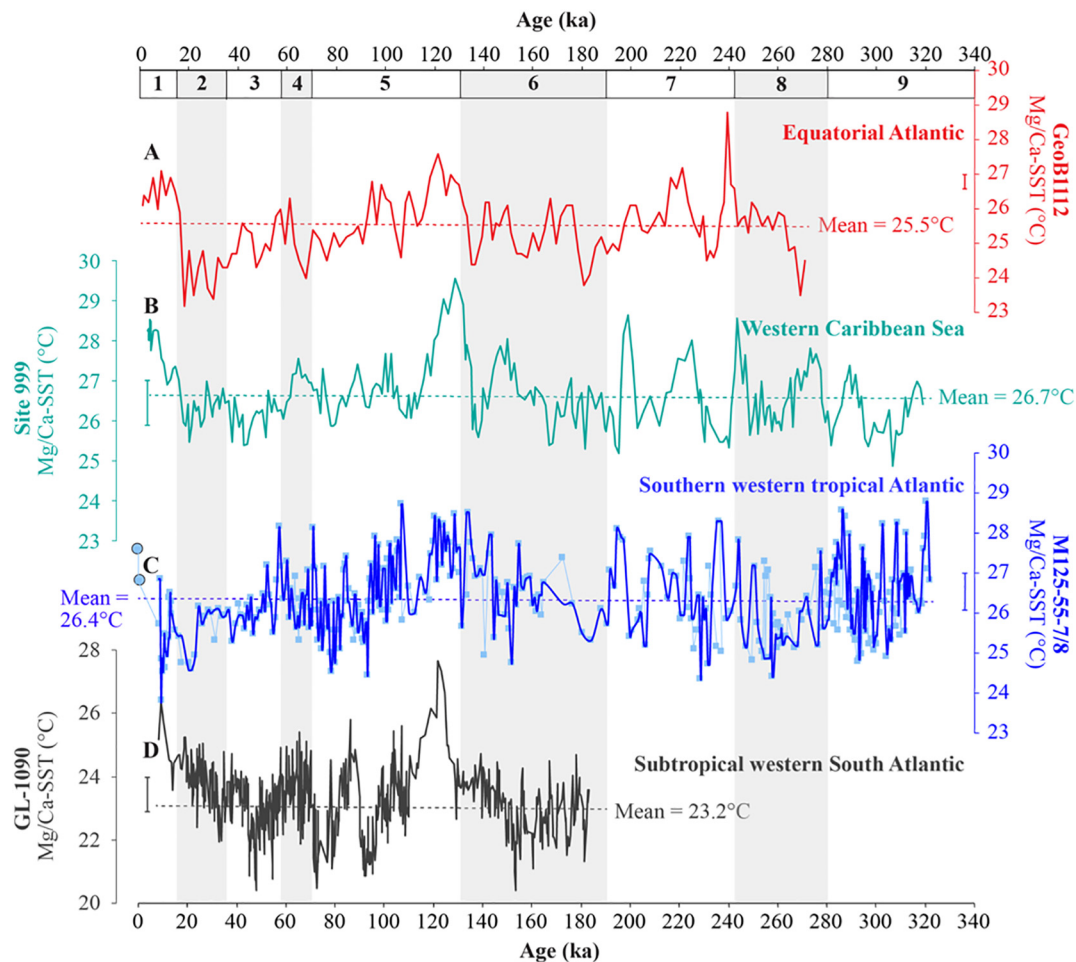


**Fig. 3.** Comparisons of sea surface temperature (SST) records from the tropical and subtropical North and South Atlantic. (A) GeoB1112 *Globigerinoides sacculifer* Mg/Ca-based SST ( $SST_{Mg/Ca}$ ) record from the equatorial Atlantic (Site 5 in Fig. 1; Nürnberg et al., 2000) (red line). (B) Site 999 *Globigerinoides ruber* (white)  $SST_{Mg/Ca}$  record from the western Caribbean Sea (Site 2 in Fig. 1 Schmidt et al., 2006) (teal line). (C) SST record based on *G. ruber* (pink) Mg/Ca ratios from Site M125-55-7 located in the western tropical South Atlantic (black star in Fig. 1). The light blue line with square markers shows the raw  $SST_{Mg/Ca}$  values and the dark blue line represents the LOESS-smoothed  $SST_{Mg/Ca}$  record (smoothing factor = 0.01). The light blue circles represent  $SST_{Mg/Ca}$  based on *G. ruber* (pink) from the parallel multicore M125-55-8. Note that four  $SST_{Mg/Ca}$  values were defined as outliers and omitted from the raw core M125-55-7  $SST_{Mg/Ca}$  data using the interquartile range. (D) GL-1090 *G. ruber* (white)  $SST_{Mg/Ca}$  record from the subtropical western South Atlantic (Site 1 in Fig. 1; Santos et al., 2017) (dark grey line). Note that GL-1090  $SST_{Mg/Ca}$  values were reduced by 15% to account for additional Mg loss during the reductive treatment of M125-55-7 *G. ruber* (Barker et al., 2003). Corresponding error bars indicating the uncertainty in  $SST_{Mg/Ca}$  values are shown adjacent to the y-axis of each SST record. SST uncertainty for core GeoB1112 is from Nürnberg et al. (2000) and SST uncertainty for cores 999 and GL-1090 are based on Dekens et al. (2002). Grey bars denote Marine Isotope Stages (MIS). (For interpretation of the references to colour in this figure legend, the reader is referred to the web version of this article.)

calibrated ages (kyr BP) using the Calib 7.10 program (Stuiver et al., 2019) (Table 1). We used the Marine13 calibration curve with a global reservoir correction of 405 years (Reimer et al., 2013). To generate benthic foraminiferal  $\delta^{18}O$  tie-points, we tuned our benthic  $\delta^{18}O_{Uvigerina}$  record to the LR04 benthic  $\delta^{18}O$  stack (Lisiecki and Raymo, 2005) (Table 2, Fig. 2a and b). The resulting age-depth model indicates that core M125-55-7 spans the past 322 kyr (Fig. 2c). The estimated uncertainty in the LR04 age model during this time period is 4 kyr, when considering all sources of uncertainty (e.g. uncertainty in the orbital solution, uncertainty in the sedimentation rate constraints, uncertainty in ice sheet response time) is 4 kyr (Lisiecki and Raymo, 2005). The average sedimentation rate is 4.0 cm/kyr with variations between 1.5 and 8.6 cm/kyr (Fig. 2c). The sampling interval of 2.5 cm thus yields an average temporal resolution of  $\sim 600$  yr for the entire time span of the record.

### 3.6. Statistics

We computed the estimated correlation coefficient and significance

between various SST records using the function “surrogateCor” implemented in the R-package ‘astrochron’ (Meyers, 2014). Prior to analysis, the data series were resampled to a common interval based on the dataset with fewer points. The estimated Pearson's correlation coefficient ( $r$ ) is based on 10,000 simulated surrogate series (see section 5.1 for results). The significance of the correlation ( $p$ ) is calculated using the method of Ebisuzaki (1997). The inter- and intrahemispheric and zonal SST gradients (see Sections 5.2.1 and 5.2.2, and Figs. 4 and 5) are Monte Carlo ensemble mean  $\Delta SST$  values based on 10,000 noisy simulations representing the combined analytical uncertainties associated with the individual SST records.

## 4. Results

The mean  $SST_{Mg/Ca}$  value over the past 322 kyr is 26.4 °C (Fig. 3c). The coldest recorded  $SST_{Mg/Ca}$  value (23.8 °C) occurred at  $\sim 9$  ka and the warmest  $SST_{Mg/Ca}$  value (28.8 °C) occurred at  $\sim 107$  ka. Our core-top data from multicore M125-55-8 yields an average modern  $SST_{Mg/Ca}$  value of 27.2 °C, which is slightly higher but still within error consistent

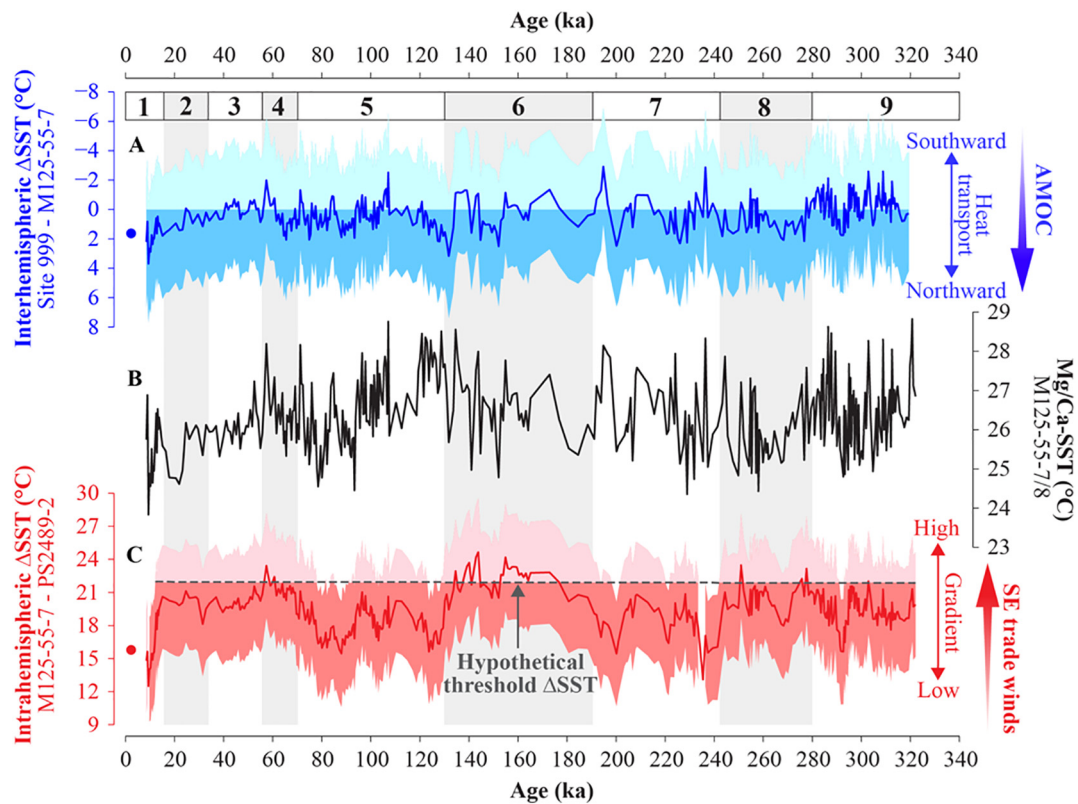


**Fig. 4.** Inter- and intrahemispheric meridional sea-surface temperature (SST) gradients. (A) Monte Carlo ensemble mean interhemispheric western tropical Atlantic (WTA) SST gradient between Site 999 (western Caribbean Sea; Site 2 in Fig. 1) (Schmidt et al., 2006) and Site M125-55-7 (southern WTA; black star in Fig. 1) (this study). Noise in the simulated gradients ( $\pm 2.1$  °C) is based on the combined analytical uncertainties of both SST records. The shaded area corresponds to the 95% confidence envelope; the light aqua shading corresponds to intervals when Site 999 SST is colder than M125-55-7 SST and the light blue shading corresponds to periods when Site 999 SST is warmer than M125-55-7 SST. The blue circle indicates the modern annual mean SST difference between Site 999 and Site M125-55-7 (Locarnini et al., 2013). (B) LOESS-smoothed M125-55-7 SST record based on *Globigerinoides ruber* (pink) Mg/Ca ratios (smoothing factor = 0.01). (C) Monte Carlo ensemble mean Southern Hemisphere SST gradient between Site M125-55-7 (southern WTA) and Site PS2489-2 (sub-Antarctic South Atlantic; Becquey and Gersonde, 2003). The PS2489-2 faunal SST record is based on the Modern Analog Technique. Noise in the simulated gradients ( $\pm 2.4$  °C) is based on the combined analytical uncertainties of both SST records. The shaded region corresponds to the 95% confidence interval. The lighter and darker pink regions correspond to intervals when the SST gradient is above and below the hypothetical threshold SST difference (dashed line; 22 °C), respectively. The red circle indicates the modern annual mean SST difference between Site 999 and Site M125-55-7 (Locarnini et al., 2013). Grey bars denote Marine Isotope Stages (MIS). (For interpretation of the references to colour in this figure legend, the reader is referred to the web version of this article.)

with the present-day mean annual SST of  $26.02 \pm 0.51$  °C at Site M125-55-7. While the M125-55-7 SST record does not display a pronounced glacial-interglacial pattern, we still broadly observe warmer SST values during interglacial periods and cooler SSTs during glacial intervals. In particular, Marine Isotope Stages (MIS) 7 and 9 appear to be well developed interglacials with warm SSTs generally above the long-term mean and MIS 4 and 8 are clearly expressed glacials with cooler SSTs mostly below the long-term mean. MIS 6 appears to be an outstanding glacial interval during which SST remained relatively warm compared to other glacial periods and displayed a conspicuous long-term increasing trend until MIS 5e, which is rather dampened in its expression.

## 5. Discussion

### 5.1. Long-term Site M125-55-7 SST evolution driven by regional processes of the WTA

To investigate whether the variability in our SST record is more sensitive to local processes of the eastern Brazilian margin or to large-scale climatic drivers of the tropical Atlantic, we compared our record to the SST record from core GL-1090 located downstream to our core site within the BC (Santos et al., 2017) and to SST records of similar time span and resolution from the western tropical North Atlantic (Site

999; western Caribbean Sea) (Schmidt et al., 2006) and the equatorial Atlantic (GeoB1112; Nürnberg et al., 2000) (Fig. 3a–d). Our comparisons indicate that relative to the neighbouring Site GL-1090 (Santos et al., 2017), SSTs at Site M125-55-7 are typically higher, with a smaller amplitude of variability (Fig. 3c and d). In addition, these two *G. ruber* Mg/Ca-based SST records display notable periods of divergent SST trends despite both sites being under the influence of the BC. A notable period of opposing SST patterns occurs during the last ~48 kyr, when the long-term warming of SSTs at Site GL-1090 coincides with a broad cooling trend at Site M125-55-7. We propose that the periodic discrepancies between SSTs at sites M125-55-7 and GL-1090 may be attributed to differences in the strength of local hydrographic processes (e.g. upwelling) and potentially differing climatic mechanisms regulating tropical and subtropical SST. It is possible that SSTs at Site GL-1090 are more strongly affected by the intrusion of cold intermediate water masses since it is closer to Cabo Frio, where upwelling is stronger than in the Vitória Upwelling System near Site M125-55-7 (Castelao and Barth, 2006; Lessa et al., 2017, 2019). Moreover, since the BC is stronger in the subtropics than the tropics (Stramma, 1989; Stramma et al., 1990), the subtropical Site GL-1090 may be more sensitive to variability in BC transport driven by changes in heat distribution between the NBC and the BC (Santos et al., 2017). Additionally, while SSTs at subtropical latitudes are strongly influenced by obliquity-driven mean annual insolation (Pahnke and Sachs, 2006), tropical Atlantic SST

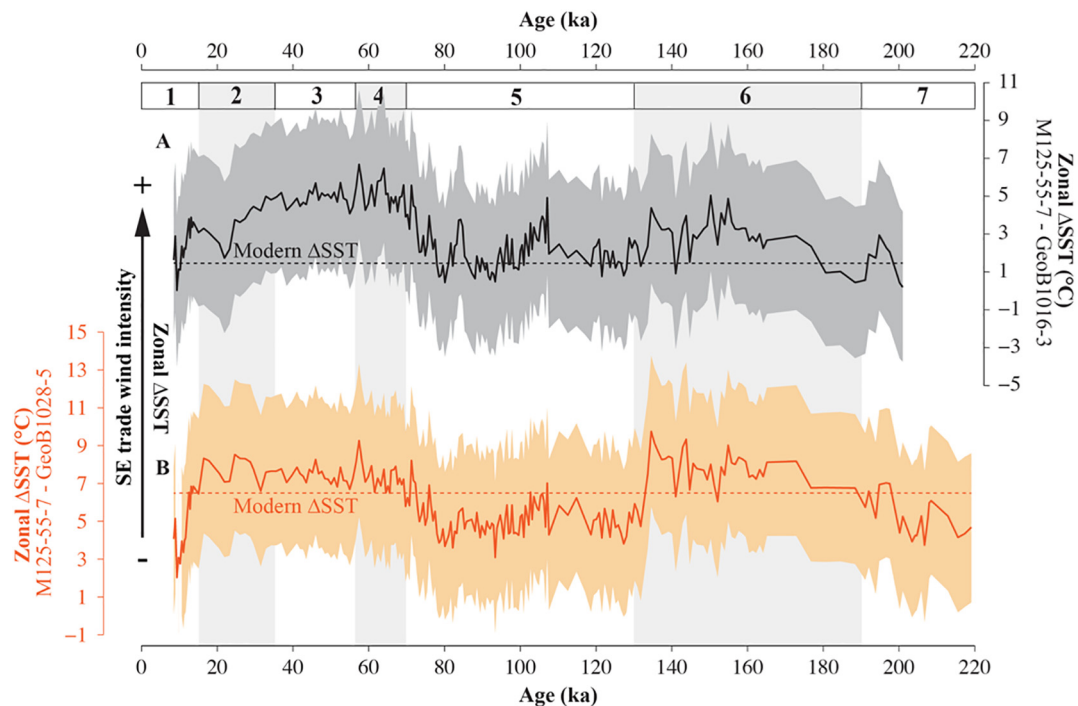


**Fig. 5.** Monte Carlo ensemble mean South Atlantic zonal sea surface temperature (SST) gradients between Site M125-55-7 (southern western tropical Atlantic) and Sites GeoB1016-3 and GeoB1028-5 located in the eastern (sub)tropical South Atlantic (Sites 3 and 4 in Fig. 1; Schneider et al., 1995). (A) Monte Carlo ensemble mean SST gradient between sites M125-55-7 and GeoB1016-3 (black line). The grey shading represents the 95% confidence envelope. Noise in the simulated gradients ( $\pm 2.0$  °C) is derived from the combined analytical uncertainties of both SST records. (B) Monte Carlo ensemble mean SST gradient between Sites M125-55-7 and GeoB1028-5 (orange line). The light orange shading corresponds to the 95% confidence interval. Noise in the simulated gradients ( $\pm 2.0$  °C) is derived from the analytical uncertainties associated with both SST records. Grey bars denote Marine Isotope Stages (MIS).

variations may be driven by other climatic variables which will be discussed in the following sections.

We find that our M125-55-7 SST record broadly resembles the long-term SST evolution at more distal sites located in the western Caribbean Sea (ODP Site 999) (Schmidt et al., 2006) and the equatorial Atlantic (GeoB1112) (Nürnberg et al., 2000) in terms of the magnitude of SST variations and mean SST over the past 322 kyr (Fig. 3a–c). In addition, the estimated correlation coefficient between the SST records from Site 999 and Site M125-55-7 reveals a weak but statistically significant long-term correlation ( $r = 0.23$ ,  $p = .035$ ). Considering this correlation and the similarities in the long-term mean SST value and the amplitude of SST variability between Site 999 and Site M125-55-7 SSTs over the past 322 kyr, we propose that the long-term variability in the M125-55-7 SST record is likely strongly influenced by large-scale climatic drivers of the entire WTA region.

## 5.2. Potential drivers of low-frequency tropical Atlantic SST variability

Since Site M125-55-7 SSTs appear to follow the thermal evolution of the WTA without notable influences from local hydrographic processes, we suggest that our record is suitable for investigating the potential climatic drivers of long-term WTA SST evolution (i.e.,  $\text{CO}_2$ , AMOC, and trade winds). While other SST records from the tropics contain dominant 100-kyr cycles and invoke eccentricity-paced  $\text{CO}_2$  forcing as the primary driver of long-term SST changes (Herbert et al., 2010; Lea, 2004; Schmidt et al., 2006), the lack of pronounced glacial/interglacial variability in our SST record suggests that direct forcing by atmospheric  $p\text{CO}_2$  is likely not the main driver of SST changes at Site M125-55-7. However, we do not argue against an indirect influence of atmospheric  $\text{CO}_2$  concentration on Site M125-55-7, potentially through modifications to the magnitude of latitudinal temperature gradients (Broccoli and Manabe, 1987) and tropical trade wind strength (Broccoli and Manabe, 1987; Mix et al., 1986; Rind, 1998) (see Section 5.2.2). In the

following sections, we investigate long-term changes in meridional and zonal heat partitioning, in order to ultimately assess the relative importance of AMOC strength and SE trade wind intensity on Site M125-55-7 SSTs.

### 5.2.1. AMOC

To evaluate whether glacial-interglacial variations in the strength of the AMOC may have contributed to the thermal evolution of the WTA, we computed a cross-equatorial WTA SST gradient between Site M125-55-7 and Site 999 from the western Caribbean Sea (Schmidt et al., 2006). This allows us to examine variations in heat distribution between the north- and southward flowing western boundary currents, and thus changes in the strength of the overturning circulation across multiple glacial-interglacial cycles. Our results show that while there are some similarities in the long-term patterns of both the interhemispheric SST gradient and the M125-55-7 SST record, the magnitude of the interhemispheric SST contrast remained low over the past 322 kyr (mean =  $0.33$  °C  $\pm 1.5$ , minimum =  $0.0$  °C  $\pm 1.5$ , maximum =  $3.7$  °C  $\pm 1.5$ ) (Fig. 4a). Since asymmetrical heat partitioning between the north- and southward-directed western boundary currents is typically due to variations in the strength of the AMOC (Chang et al., 1997; Dahl et al., 2005; Vellinga and Wood, 2002; Yang, 1999), the consistently low interhemispheric SST contrast suggests that changes to the strength of the AMOC are unlikely to be the dominant driver of SST changes in the WTA. It should be noted that since the resolution of our SST gradient does not capture millennial-scale SST variability in the WTA, it does not preclude a sensitivity of the WTA to abrupt and major changes in AMOC strength during Heinrich Stadials.

### 5.2.2. SE trade winds

We computed zonal SST gradients between Site M125-55-7 and two sites in the eastern tropical South Atlantic (GeoB1016-3 and GeoB1028-5) (Schneider et al., 1995) to examine the long-term evolution of east-

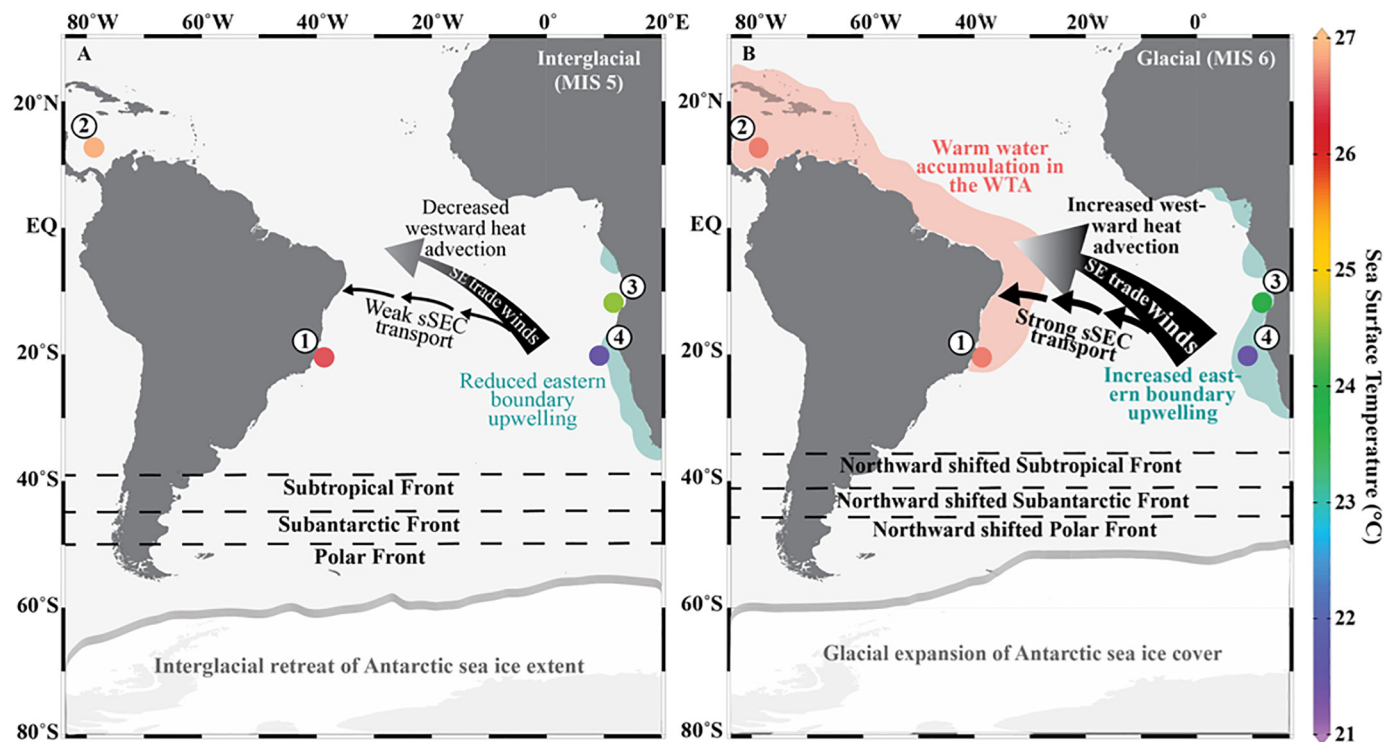


**Fig. 6.** Schematic diagram illustrating the proposed mechanism of sea surface temperature (SST) forcing and surface-heat distribution in the tropical Atlantic. (A) Interglacial configuration: southward retreat of Antarctic sea-ice extent, poleward displacement of the Southern Ocean frontal systems, weakening of the southeast (SE) trades. The relaxation of the SE trade winds reduces eastern boundary upwelling and also decreases westward heat advection within the sSEC. This results in a small east-west SST contrast during interglacials. Colored dots correspond to mean MIS 5 SST at sites (1) M125-55-7, (2) ODP999A (Schmidt et al., 2006), (3) GeoB1016-3 (Schneider et al., 1995) and (4) GeoB1028-5 (Schneider et al., 1995). See colour bar on the left for the respective SST ranges. (B) Glacial configuration: expansion of Antarctic sea-ice cover, northward shift of Southern Ocean fronts, intensification of the SE trades. The glacially strengthened SE trade winds promote strong upwelling along the eastern boundary and enhance the westward advection of heat by the sSEC. This causes warm waters to pile up in the WTA creating a strong east-west SST contrast. Colored dots correspond to mean MIS 6 SST at sites: (1) M125-55-7, (2) ODP999A (Schmidt et al., 2006), (3) GeoB1016-3 (Schneider et al., 1995) and (4) GeoB1028-5 (Schneider et al., 1995). This figure was produced with Ocean Data View (Schlitzer, 2018).

west heat distribution within the (sub) tropical South Atlantic (Fig. 5). Compared to the computed meridional SST gradient, the magnitude of the computed zonal temperature gradients between Site M125-55-7 and the eastern tropical South Atlantic sites are considerably greater (GeoB1016-3: mean = 3.0 °C, minimum = 0.0 °C, maximum = 6.7 °C; GeoB1028-5: mean = 6.1 °C, minimum = 2.0 °C, maximum = 9.8 °C). Unlike the interhemispheric temperature gradient, the zonal SST contrasts displays high-amplitude glacial-interglacial variability. During interglacials (e.g. MIS 7, MIS 5, Holocene), the east-west thermal gradient is relatively low, while during glacial periods (e.g. MIS 6, MIS 4–2) the thermal gradient is enhanced. We propose that the variations in the magnitude of the zonal thermal gradient between the eastern and western tropical South Atlantic may be driven by glacial-interglacial fluctuations in the strength of the SE trade winds (Little et al., 1997a, 1997b; Stuu et al., 2002). During glacial periods when atmospheric  $p\text{CO}_2$  is low and circum-Antarctic sea-ice extent is expanded, the SE trade winds are intensified due to the compression of the tropical atmospheric circulation cell by the combined influence of a high hemispheric thermal gradient and equatorward displaced Southern Ocean frontal systems (Kim and Schneider, 2003; Mix and Morey, 1996; Mix et al., 1986; Stuu et al., 2002). The glacially-intensified SE trade winds induce intense upwelling of cold SACW off the coast of South Africa and Namibia (Kim and Schneider, 2003; Kim et al., 2003; Little et al., 1997a, 1997b) and strengthen the westward advection of heat within the sSEC (Merle, 1980). This accumulation of warm waters in the western tropics deepens the thermocline and causes further warming in the WTA due to the decrease in vertical heat flux out of the surface layer (Hastenrath and Merle, 1987; Merle, 1980; Venancio et al., 2018; Wolff et al., 1999). Thus, the glacial strengthening of the SE trade winds

produces a large zonal SST contrast within the southern WTA (Fig. 6b). During interglacial periods when atmospheric  $p\text{CO}_2$  is high and Antarctic sea ice is retreated further to the south, the reduction of the meridional temperature gradient and poleward displacement of the Southern Ocean fronts causes the SE trade winds to weaken (Kim and Schneider, 2003; McIntyre et al., 1989; Mix and Morey, 1996; Stuu et al., 2002). The relaxation of the SE trade winds reduces eastern boundary upwelling (Kim and Schneider, 2003; Kim et al., 2003; Little et al., 1997a, 1997b) and decreases westward heat advection via the sSEC (Merle, 1980). The subsequent shoaling of the thermocline in the southern WTA enhances vertical heat flux out of the upper mixed layer, contributing further to surface cooling in the western basin (Merle, 1980; Venancio et al., 2018; Wolff et al., 1999). Therefore, interglacial weakening of the SE trade winds weakens the east-west thermal contrast within the tropical South Atlantic Ocean (Fig. 6a).

To determine whether SE trade wind intensity had an exceptionally strong influence on WTA SST during the MIS 6 prolonged warming interval, we computed a 322-kyr record of the Southern Hemisphere SST gradient between the tropics and the subantarctic zone using the SST record from Core PS2489 (42°52.4'S, 8°58.4'E; Becquey and Gersonde, 2003) and our M125-55-7 tropical SST record (mean = 19.4 °C, minimum = 12.5, maximum = 24.7) (Fig. 4c). Since trade wind strength is dependent on the thermal gradient of its hemisphere of origin (Rind, 1998), this intra-hemispheric SST gradient may provide an approximation of the intensity of the SE trades (Wolff et al., 1999). Based on this computed gradient, we propose that the high intra-hemispheric SST gradient sustained throughout MIS 6 may have led to an exceptional intensification of the SE trades. As discussed in the previous paragraph, a strengthening of the SE trade winds increases

westward heat advection via the sSEC (Merle, 1980) resulting in warming in the WTA due to the buildup of warm water masses and deepening of the thermocline (Hastenrath and Merle, 1987; Merle, 1980; Venancio et al., 2018; Wolff et al., 1999). We hypothesize that if the intra-hemispheric temperature gradient is sustained above a threshold for a prolonged interval, as may have been the case during MIS 6, exceptionally strong SE trades may have a dominant influence on SSTs in the WTA (Fig. 4c).

## 6. Conclusions

Our SST record from Site M125-55-7 indicates that the surface mixed layer of the southern WTA experienced low-amplitude variations with generally warm tropical temperatures over the past 322 kyr. The similarity between our SST record and the SST record from Site 999 (western Caribbean Sea) indicates that Site M125-55-7 is influenced by regional processes driving the thermal evolution of the WTA. Based on the lack of clear glacial-interglacial variability in our record, we propose that atmospheric  $pCO_2$  is likely not a significant direct driver of long-term WTA SST variations, although its indirect effects cannot be excluded. Our results indicate that variability in the intrahemispheric latitudinal SST gradient and the associated changes in the intensity of the SE trades may have produced the observed variability in southern WTA SSTs over the past 322 kyr. We suggest that an increase in the magnitude of the intrahemispheric temperature gradient and a subsequent intensification of the SE trade winds likely produced the anomalous SST warming pattern during MIS 6. The low variability in the interhemispheric SST contrast between the northern and southern WTA over the past 322 kyr suggests that variations in the strength of the AMOC did not significantly influence long-term WTA SST. More pronounced, however, are the variations of the zonal SST contrast between Site M125-55-7 and the eastern tropical South Atlantic localities. We propose that the glacial amplification of the east-west thermal gradient is caused by an intensification of the SE trade winds, whereas the diminished SST contrast during interglacial intervals reflects weaker SE trade winds. As such, this study highlights the sensitivity of WTA SST and the zonal South Atlantic temperature gradient to fluctuations in the strength of the SE trade winds.

## Data availability

The original data reported in this paper is archived in Pangaea (<https://doi.pangaea.de/10.1594/PANGAEA.905301>).

## Declaration of Competing Interest

None.

## Acknowledgements

We kindly acknowledge the support by captain and crew of the R/V METEOR during expedition M125. We thank Bernd Knape and Christian Scholz for assistance with stable isotope and ICP-OES analyses, respectively. Andrea Jaeschke provided important contributions during manuscript preparation. We are grateful to the S. Szidat and the LARA team at the University of Bern for providing the  $^{14}C$  dates. AB was funded by the Deutsche Forschungsgemeinschaft (DFG) via Grant BA 3809/9-1. CMC acknowledges the financial support from FAPESP (grants 2018/15123-4), CAPES (grants 564/2015 and 88881.313535/2019-01), CNPq (grants 302607/2016-1 and 422255/2016-5) and the Alexander von Humboldt Foundation, Germany.

## References

Aguiar, A.L., Cirano, M., Pereira, J., Marta-Almeida, M., 2014. Upwelling processes along a western boundary current in the Abrolhos-Campos region of Brazil. *Cont. Shelf Res.*

- 85, 42–59. <https://doi.org/10.1016/j.csr.2014.04.013>.
- Arz, H.W., Pätzold, J., Wefer, G., 1999. The deglacial history of the western tropical Atlantic as inferred from high resolution stable isotope records off northeastern Brazil. *Earth Planet. Sci. Lett.* 167 (1–2), 105–117. [https://doi.org/10.1016/S0012-821X\(99\)00025-4](https://doi.org/10.1016/S0012-821X(99)00025-4).
- Bahr, A., Albuquerque, A.L.S., Ardenghi, N., Batenburg, S.J., Bayer, M., Catunda, M.C., Conforti, A., et al., 2016. South American Hydrological Balance and Paleooceanography during the Late Pleistocene and Holocene (SAMBA) – Cruise No. M125 – March 21 – April 15, 2016 - Rio de Janeiro (Brazil) – Fortaleza (Brazil). METEOR-Berichte, M125, 47 pp. DFG-Senatskommission für Ozeanographie. [https://doi.org/10.2312/cr\\_m125](https://doi.org/10.2312/cr_m125).
- Bard, E., Rostek, F., Turon, J.L., Gendreau, S., 2000. Hydrological impact of Heinrich events in the subtropical Northeast Atlantic. *Science* 289 (5483), 1321–1324. <https://doi.org/10.1126/science.289.5483.1321>.
- Barker, S., Greaves, M., Elderfield, H., 2003. A study of cleaning procedures used for foraminiferal Mg/Ca paleothermometry. *Geochem. Geophys. Geosyst.* 4 (9), 1–20.
- Becquey, S., Gersonde, R., 2003. A 0.55-Ma paleotemperature record from the sub-antarctic zone: implications for Antarctic circumpolar current development. *Paleoceanography* 18 (1), 1014. <https://doi.org/10.1029/2000PA000576>.
- Böhm, E., Lippold, J., Gutjahr, M., Frank, M., Blaser, P., Antz, B., Fohlmeister, J., et al., 2015. Strong and deep Atlantic meridional overturning circulation during the last glacial cycle. *Nature* 517 (7532), 73–76. <https://doi.org/10.1038/nature14059>.
- Broccoli, A.J., Manabe, S., 1987. The influence of continental ice, atmospheric  $CO_2$ , and land albedo on the climate of the last glacial maximum. *Clim. Dyn.* 1 (2), 87–99. <https://doi.org/10.1007/BF01054478>.
- Campos, E.J.D., Lorenzetti, J.A., Stevenson, M.R., Stech, J.L., De Souza, R.B., 1996. Penetration of waters from the Brazil-Malvinas confluence region along the South American continental shelf up to 23°S. *An. Acad. Bras. Cienc.* 68 (Suppl. 1), 57–58.
- Carton, J.A., Huang, G., 1994. Warm events in the tropical Atlantic. *J. Phys. Oceanogr.* 24, 888–903. [https://doi.org/10.1175/1520-0485\(1994\)024<0888:WEITTA>2.0.CO;2](https://doi.org/10.1175/1520-0485(1994)024<0888:WEITTA>2.0.CO;2).
- Carton, J.A., Zhou, Z., 1997. Annual cycle of sea surface temperature in the tropical Atlantic Ocean. *J. Geophys. Res.* 102 (C13), 27813–27824. <https://doi.org/10.1029/97JC02197>.
- Castelao, R.M., Barth, J.A., 2006. Upwelling around Cabo Frio, Brazil: the importance of wind stress curl. *Geophys. Res. Lett.* 33 (3), L03602. <https://doi.org/10.1029/2005GL025182>.
- Castro, B.M., Brandini, F.P., Pires-Vanin, A.M.S., de Miranda, L.B., 2006. Multidisciplinary oceanographic processes on the Western Atlantic Continental Shelf between 4°N and 34°S. *Sea 14A (April 2016)*, 259–294 Volume 14A: The Global Coastal Ocean.
- Chang, P., Ji, L., Li, H., 1997. A decadal climate variation in the tropical Atlantic Ocean from thermodynamic air-sea interactions. *Nature* 385 (6616), 516–518. <https://doi.org/10.1038/385516a0>.
- Chiessi, C.M., Ulrich, S., Multiza, S., Pätzold, J., Wefer, G., 2007. Signature of the Brazil-Malvinas Confluence (Argentine Basin) in the isotopic composition of planktonic foraminifera from surface sediments. *Mar. Micropaleontol.* 64, 52–66. <https://doi.org/10.1016/j.marmicro.2007.02.002>.
- Chiessi, C.M., Multiza, S., Mollenhauer, G., Silva, J.B., Groeneveld, J., Prange, M., 2015. Thermal evolution of the western South Atlantic and the adjacent continent during Termination 1. *Clim. Past* 11 (6), 915–929. <https://doi.org/10.5194/cp-11-915-2015>.
- Dahl, K.A., Broccoli, A.J., Stouffer, R.J., 2005. Assessing the role of North Atlantic freshwater forcing in millennial scale climate variability: a tropical Atlantic perspective. *Clim. Dyn.* 24 (4), 325–346. <https://doi.org/10.1007/s00382-004-0499-5>.
- Dekens, P.S., Lea, D.W., Pak, D.K., Spero, H.J., 2002. Core top calibration of Mg/Ca in tropical foraminifera: refining paleotemperature estimation. *Geochem. Geophys. Geosyst.* 3 (4), 1–29. <https://doi.org/10.1029/2001GC000200>.
- Ebisuzaki, W., 1997. A method to estimate the statistical significance of a correlation when the data are serially correlated. *Am. Meteorol. Soc.* 10, 2147–2153. [https://doi.org/10.1175/1520-0442\(1997\)010%3C2147:AMTETS%3E2.0.CO;2](https://doi.org/10.1175/1520-0442(1997)010%3C2147:AMTETS%3E2.0.CO;2).
- Elderfield, H., Vautravers, M., Cooper, M., 2002. The relationship between shell size and Mg/Ca, Sr/Ca,  $\delta^{18}O$ , and  $\delta^{13}C$  of species of planktonic foraminifera. *Geochem. Geophys. Geosyst.* 3 (8), 1–13. <https://doi.org/10.1029/2001gc000194>.
- Franchito, S.H., Oda, T.O., Rao, V.B., Kayano, M.T., 2008. Interaction between coastal upwelling and local winds at Cabo Frio, Brazil: an observational study. *J. Appl. Meteorol. Climatol.* 47 (6), 1590–1598. <https://doi.org/10.1175/2007JAMC1660.1>.
- Friedrich, O., Schiebel, R., Wilson, P.A., Weldeab, S., Beer, C.J., Cooper, M.J., Fiebig, J., 2012. Influence of test size, water depth, and ecology on Mg/Ca, Sr/Ca,  $\delta^{18}O$  and  $\delta^{13}C$  in nine modern species of planktic foraminifera. *Earth Planet. Sci. Lett.* 319–320, 133–145. <https://doi.org/10.1016/j.epsl.2011.12.002>.
- Gottschalk, J., Szidat, S., Michel, E., Mazaud, A., Salazar, G., Battaglia, M., Lippold, J., Jaccard, S.L., 2018. Radiocarbon measurements of small-size foraminiferal samples with the Mini CArbon Dating System (MICADAS) at the University of Bern: implications for paleoclimate reconstructions. *Radiocarbon* 60 (2), 469–491. <https://doi.org/10.1017/RDC.2018.3>.
- Hastenrath, S., 1980. Heat budget of tropical ocean and atmosphere. *J. Phys. Oceanogr.* 10 (2), 159–170. [https://doi.org/10.1175/1520-0485\(1980\)010<0159:hboota>2.0.co;2](https://doi.org/10.1175/1520-0485(1980)010<0159:hboota>2.0.co;2).
- Hastenrath, S., Merle, J., 1987. Annual cycle of subsurface thermal structure in the Tropical Atlantic Ocean. *J. Phys. Oceanogr.* 17 (9), 1518–1538. [https://doi.org/10.1175/1520-0485\(1987\)017<1518:acosts>2.0.co;2](https://doi.org/10.1175/1520-0485(1987)017<1518:acosts>2.0.co;2).
- Herbert, T.D., Peterson, L.C., Lawrence, K.T., Liu, Z., 2010. Tropical Ocean temperatures over the past 3.5 million years. *Science* 328 (5985), 1530–1534. <https://doi.org/10.1126/science.1185435>.
- Johns, W.E., Lee, T.N., Beardsley, R.C., Candela, J., Limeburner, R., Castro, B., 2002.

- Annual cycle and variability of the North Brazil current. *J. Phys. Oceanogr.* 28 (1), 103–128. [https://doi.org/10.1175/1520-0485\(1998\)028<0103:acavot>2.0.co;2](https://doi.org/10.1175/1520-0485(1998)028<0103:acavot>2.0.co;2)
- Kim, J.H., Schneider, R.R., 2003. Low-latitude control of interhemispheric sea-surface temperature contrast in the tropical Atlantic over the past 21 kyr: the possible role of SE trade winds. *Clim. Dyn.* 21 (3–4), 337–347. <https://doi.org/10.1007/s00382-003-0341-5>.
- Kim, J.H., Schneider, R.R., Mulitza, S., Müller, P.J., 2003. Reconstruction of SE trade-wind intensity based on sea-surface temperature gradients in the Southeast Atlantic over the last 25 kyr. *Geophys. Res. Lett.* 30 (22). <https://doi.org/10.1029/2003GL017557>.
- Lea, D.W., 2004. The 100 000-yr cycle in tropical SST, greenhouse forcing, and climate sensitivity. *J. Clim.* 17 (11), 2170–2179. [https://doi.org/10.1175/1520-0442\(2004\)017<2170:TYCITS>2.0.CO;2](https://doi.org/10.1175/1520-0442(2004)017<2170:TYCITS>2.0.CO;2).
- Lessa, D.V.O., Santos, T.P., Venancio, I.M., Albuquerque, A.L.S., 2017. Offshore expansion of the Brazilian coastal upwelling zones during Marine Isotope Stage 5. *Glob. Planet. Chang.* 158, 13–20. <https://doi.org/10.1016/j.gloplacha.2017.09.006>.
- Lessa, D.V.O., Santos, T.P., Venancio, I.M., Santarosa, A.C.A., dos Santos Junior, E.C., Toledo, F.A.L., Costa, K.B., Albuquerque, A.L.S., 2019. Eccentricity-induced expansions of Brazilian coastal upwelling zones. *Glob. Planet. Chang.* 179, 33–42. <https://doi.org/10.1016/j.gloplacha.2019.05.002>.
- Lisiecki, L.E., Raymo, M.E., 2005. A Pliocene-Pleistocene stack of 57 globally distributed benthic  $\delta^{18}\text{O}$  records. *Paleoceanography* 20 (1), 1–17. <https://doi.org/10.1029/2004PA001071>.
- Little, M.G., Schneider, R.R., Kroon, D., Price, B., Bickert, T., Wefer, G., 1997a. Rapid palaeoceanographic changes in the Benguela Upwelling System for the last 160,000 years as indicated by abundances of planktonic foraminifera. *Palaeogeogr. Palaeoclimatol. Palaeoecol.* 130 (1–4), 135–161. [https://doi.org/10.1016/S0031-0182\(96\)00136-8](https://doi.org/10.1016/S0031-0182(96)00136-8).
- Little, M.G., Schneider, R.R., Kroon, D., Price, B., Summerhayes, C.P., Segl, M., 1997b. Trade wind forcing of upwelling, seasonality, and Heinrich events as a response to sub-Milankovitch climate variability. *Paleoceanography* 12 (4), 568–576. <https://doi.org/10.1029/97PA00823>.
- Locarnini, R.A., Mishonov, A.V., Antonov, J.I., Boyer, T.P., Garcia, H.E., Baranova, O.K., Zweng, M.M., et al., 2013. In: Levitus, S. (Ed.), *World Ocean Atlas 2013, Volume 1: Temperature*. NOAA Atlas NESDIS 73 A. Mishonov Technical Ed., 40 pp.
- Marengo, J.A., Bernasconi, M., 2015. Regional differences in aridity/drought conditions over Northeast Brazil: present state and future projections. *Clim. Chang.* 129 (1–2), 103–115. <https://doi.org/10.1007/s10584-014-1310-1>.
- Martin, P.A., Lea, D.W., 2002. A simple evaluation of cleaning procedures on fossil benthic foraminiferal Mg/Ca. *Geochem. Geophys. Geosyst.* 3 (10), 1–8. <https://doi.org/10.1029/2001GC000280>.
- McIntyre, A., Ruddiman, W.F., Karlin, K., Mix, A.C., 1989. Surface water response of the equatorial Atlantic Ocean to orbital forcing. *Paleoceanography* 4 (1), 19–55. <https://doi.org/10.1029/PA0041001p00019>.
- Merle, J., 1980. Seasonal heat budget in the equatorial Atlantic Ocean. *J. Phys. Oceanogr.* 10 (3), 464–469. [https://doi.org/10.1175/1520-0485\(1980\)010<0464:shbite>2.0.co;2](https://doi.org/10.1175/1520-0485(1980)010<0464:shbite>2.0.co;2).
- Meyers, S.R., 2014. Astrochron: An R Package for Astrochronology. <https://cran.r-project.org/package=astrochron>.
- Mix, A.C., Morey, A.E., 1996. Climate feedback and Pleistocene variations in the Atlantic South Equatorial current. In: *The South Atlantic, Present and Past Circulation*, pp. 503–525. [https://doi.org/10.1007/978-3-642-80353-6\\_26](https://doi.org/10.1007/978-3-642-80353-6_26).
- Mix, A.C., Ruddiman, W.F., McIntyre, A., 1986. Late Quaternary paleoceanography of the Tropical Atlantic, 1: spatial variability of annual mean sea-surface temperatures, 0–20,000 years B.P. *Paleoceanography* 1 (1), 43–66. <https://doi.org/10.1029/PA001i001p00043>.
- Molinari, R.L., 1983. Observations of near-surface currents and temperature in the central and western tropical Atlantic Ocean. *J. Geophys. Res.* 88 (C7), 4433–4438. <https://doi.org/10.1029/JC088iC07p04433>.
- Mulitza, S., Chiessi, C.M., Schefuß, E., Lippold, J., Wichmann, D., Antz, B., Mackensen, A., et al., 2017. Synchronous and proportional deglacial changes in Atlantic meridional overturning and northeast Brazilian precipitation. *Paleoceanography* 32 (6), 622–633. <https://doi.org/10.1002/2017PA003084>.
- Nürnberg, D., Müller, A., Schneider, R.R., 2000. Paleo-sea surface temperature calculations in the equatorial East Atlantic from Mg/Ca ratios in planktic foraminifera: a comparison to sea surface temperature estimates from  $\text{U}^{37}\text{K}$ , oxygen isotopes, and foraminiferal transfer function. *Paleoceanography* 15 (1), 124–134. <https://doi.org/10.1029/1999PA000370>.
- Pahnke, K., Sachs, J.P., 2006. Sea surface temperatures of southern midlatitudes 0–160 kyr B.P. *Paleoceanography* 21, 1–17. <https://doi.org/10.1029/2005PA001191>.
- Paillard, D., Labeyrie, L., Yiou, P., 1996. Macintosh Program performs time-series analysis. *Eos, Trans. AGU* 77, 379.
- Peterson, R.G., Stramma, L., 1991. Upper-level circulation in the South Atlantic Ocean. *Prog. Oceanogr.* 26, 1–73. [https://doi.org/10.1016/0079-6611\(91\)90006-8](https://doi.org/10.1016/0079-6611(91)90006-8).
- Reimer, P.J., Bard, E., Bayliss, A., Beck, J.W., Blackwell, P.G., Ramsey, C.B., Buck, C.E., et al., 2013. *IntCal13 and Marine13 radiocarbon age calibration curves 0–50,000 years cal BP*. *Radiocarbon* 55 (4), 1869–1887.
- Rind, D., 1998. Latitudinal temperature gradients and climate change. *J. Geophys. Res. Atmos.* 103 (D6), 5943–5971. <https://doi.org/10.1029/97JD03649>.
- Rodrigues, R.R., Lorenzetti, J.A., 2001. A numerical study of the effects of bottom topography and coastline geometry on the Southeast Brazilian coastal upwelling. *Cont. Shelf Res.* 21 (4), 371–394. [https://doi.org/10.1016/S0278-4343\(00\)0094-7](https://doi.org/10.1016/S0278-4343(00)0094-7).
- Rodrigues, R.R., Rothstein, L.M., Wimbush, M., 2007. Seasonal variability of the South Equatorial Current bifurcation in the Atlantic Ocean: a numerical study. *J. Phys. Oceanogr.* 37 (1), 16–30. <https://doi.org/10.1175/jpo2983.1>.
- Rühlemann, C., Mulitza, S., Müller, P.J., Wefer, G., Zahn, R., 1999. Warming of the tropical Atlantic Ocean and slowdown of thermohaline circulation during the last deglaciation. *Nature* 402 (6761), 511–514. <https://doi.org/10.1038/990069>.
- Santos, T.P., Lessa, D.O., Venancio, I.M., Chiessi, C.M., Mulitza, S., Kuhnert, H., Govin, A., et al., 2017. Prolonged warming of the Brazil current precedes deglaciations. *Earth Planet. Sci. Lett.* 463, 1–12. <https://doi.org/10.1016/j.epsl.2017.01.014>.
- Schlitzer, R., 2018. Ocean Data View. <http://odv.awi.de>.
- Schmid, C., Majumder, S., 2018. Transport variability of the Brazil current from observations and a data assimilation model. *Ocean Sci.* 14 (3), 417–436. <https://doi.org/10.5194/os-14-417-2018>.
- Schmid, C., Schäfer, H., Zenk, W., Podestá, G., 2002. The Vitória Eddy and its relation to the Brazil current. *J. Phys. Oceanogr.* 25 (11), 2532–2546. [https://doi.org/10.1175/1520-0485\(1995\)025<2532:tveair>2.0.co;2](https://doi.org/10.1175/1520-0485(1995)025<2532:tveair>2.0.co;2).
- Schmidt, M.W., Spero, H.J., Vautravers, M.J., 2006. Western Caribbean Sea surface temperatures during the late Quaternary. *Geochem. Geophys. Geosyst.* 7 (2). <https://doi.org/10.1029/2005GC000957>.
- Schneider, R.R., Müller, P.J., Ruhlmann, G., 1995. Late Quaternary surface circulation in the east equatorial South Atlantic: evidence from Alkenone Sea surface temperatures. *Paleoceanography* 10 (2), 197–219. <https://doi.org/10.1029/94PA03308>.
- Shannon, L.V., Nelson, G., 1996. The Benguela: large scale features and processes and system variability. In: *The South Atlantic, Present and Past Circulation*, pp. 163–210. [https://doi.org/10.1007/978-3-642-80353-6\\_9](https://doi.org/10.1007/978-3-642-80353-6_9).
- Shi, N., Schneider, R., Beug, H.J., Dupont, L.M., 2001. Southeast trade wind variations during the last 135 kyr: evidence from pollen spectra in eastern South Atlantic sediments. *Earth Planet. Sci. Lett.* 187 (3–4), 311–321. [https://doi.org/10.1016/S0012-821X\(01\)00267-9](https://doi.org/10.1016/S0012-821X(01)00267-9).
- Steph, S., Regenberg, M., Tiedemann, R., Mulitza, S., Nürnberg, D., 2009. Stable isotopes of planktonic foraminifera from tropical Atlantic/Caribbean core-tops: Implications for reconstructing upper ocean stratification. *Mar. Micropaleontol.* 71 (1–2), 1–19. <https://doi.org/10.1016/j.marmicro.2008.12.004>.
- Stramma, L., 1989. The Brazil current transport south of 23°S. *Deep Sea Res. Part A Oceanogr. Res. Papers* 36 (4), 639–646. [https://doi.org/10.1016/0198-0149\(89\)90012-5](https://doi.org/10.1016/0198-0149(89)90012-5).
- Stramma, L., 1991. Geostrophic transport of the South Equatorial current in the Atlantic. *J. Mar. Res.* 49 (2), 281–294. <https://doi.org/10.1357/002224091784995864>.
- Stramma, L., England, M., 1999. On the water masses and mean circulation of the South Atlantic Ocean. *J. Geophys. Res. Oceans* 104 (C9), 20863–20883. <https://doi.org/10.1029/1999jc900139>.
- Stramma, L., Ikeda, Y., Peterson, R.G., 1990. Geostrophic transport in the Brazil current region north of 20°S. *Deep Sea Res. Part A Oceanogr. Res. Papers* 37 (12), 1875–1886. [https://doi.org/10.1016/0198-0149\(90\)90083-8](https://doi.org/10.1016/0198-0149(90)90083-8).
- Stuiver, M., Reimer, P.J., Reimer, R.W., 2019. CALIB 7.1 [WWW program] at. <http://calib.org>. Accessed date: 26 August 2019.
- Stuut, J.B.W., Prins, M.A., Schneider, R.R., Weltje, G.J., Fred Jansen, J.H., Postma, G., 2002. A 300-kyr record of aridity and wind strength in southwestern Africa: inferences from grain-size distributions of sediments on Walvis Ridge, SE Atlantic. *Mar. Geol.* 180 (1–4), 221–233. [https://doi.org/10.1016/S0025-3227\(01\)00215-8](https://doi.org/10.1016/S0025-3227(01)00215-8).
- Szidat, S., Salazar, G.A., Vogel, E., Battaglia, M., Wacker, L., Synal, H.-A., Türlér, A., 2014.  $^{14}\text{C}$  analysis and sample preparation at the new Bern Laboratory for the Analysis of Radiocarbon with AMS (LARA). *Radiocarbon* 56 (2), 561–566. <https://doi.org/10.2458/56.17457>.
- Tolderlund, D.S., Bé, A.W.H., 1971. Seasonal distribution of Planktonic Foraminifera in the Western North Atlantic. *Micropaleontology* 17 (3), 297–329. <https://doi.org/10.2307/1485143>.
- Vellinga, M., Wood, R.A., 2002. Global climatic impacts of a collapse of the Atlantic thermohaline circulation. *Clim. Chang.* 54 (3), 251–267. <https://doi.org/10.1023/A:1016168827653>.
- Venancio, I.M., Mulitza, S., Govin, A., Santos, T.P., Lessa, D.O., Albuquerque, A.L.S., Chiessi, C.M., et al., 2018. Millennial- to orbital-scale responses of Western Equatorial Atlantic thermocline depth to changes in the trade wind system since the last interglacial. *Paleoceanogr. Paleoclimatol.* 33 (12), 1490–1507. <https://doi.org/10.1029/2018PA003437>.
- Wang, X., Auler, A.S., Edwards, L.L., Cheng, H., Cristalli, P.S., Smart, P.L., Richards, D.A., et al., 2004. Wet periods in northeastern Brazil over the past 210 kyr linked to distant climate anomalies. *Nature* 432 (7018), 740–743. <https://doi.org/10.1038/nature03067>.
- Weldeab, S., Schneider, R.R., Kölling, M., 2006. Deglacial Sea surface temperature and salinity increase in the western tropical Atlantic in synchrony with high latitude climate instabilities. *Earth Planet. Sci. Lett.* 241 (3–4), 699–706. <https://doi.org/10.1016/j.epsl.2005.11.012>.
- Wolff, T., Mulitza, S., Rühlemann, C., Wefer, G., 1999. Response of the tropical Atlantic thermocline to Late Quaternary trade wind changes. *Paleoceanography* 14 (3), 374–383. <https://doi.org/10.1029/1999PA000111>.
- Yang, J., 1999. A linkage between decadal climate variations in the Labrador Sea and the tropical Atlantic Ocean. *Geophys. Res. Lett.* 26 (8), 1023–1026. <https://doi.org/10.1029/1999GL900181>.
- Zweng, M.M., Reagan, J.R., Antonov, J.I., Locarnini, R.A., Mishonov, A.V., Boyer, T.P., Garcia, H.E., et al., 2013. In: S. Levitus, A. Mishonov (Eds.), *World Ocean Atlas. Salinity 2*. pp. 39 NOAA Atlas NESDIS 74.